arXiv:0810.4013v1 [cond-mat.str-el] 22 Oct 2008

Exchange bias effect in the phase separated $Nd_{1-x}Sr_xCoO_3$ at the spontaneous ferromagnetic/ferrimagnetic interface

M. Patra, M. Thakur, S. Majumdar and S. Giri*
Department of Solid State Physics and Center for Advanced Materials,
Indian Association for the Cultivation of Science, Jadavpur, Kolkata 700 032, INDIA

We report the new results of exchange bias effect in $Nd_{1-x}Sr_xCoO_3$ for $x = 0.20$ and 0.40, where the exchange bias phenomenon is involved with the ferrimagnetic (FI) state in a spontaneously phase separated system. The zero-field cooled magnetization exhibits the FI (T_{FI}) and ferromagnetic (T_C) transitions at ~ 23 and ~ 70 K, respectively for $x = 0.20$. The negative horizontal and positive vertical shifts of the magnetic hysteresis loops are observed when the system is cooled through T_{FI} in presence of a positive static magnetic field. Training effect is observed for $x = 0.20$, which could be interpreted by a spin configurational relaxation model. The unidirectional shifts of the hysteresis loops as a function of temperature exhibit the absence of exchange bias above T_{FI} for $x = 0.20$. The analysis of the cooling field dependence of exchange bias field and magnetization indicates that the ferromagnetic (FM) clusters consist of single magnetic domain with average size around ~ 20 and ~ 40 Å for $x = 0.20$ and 0.40, respectively. The sizes of the FM clusters are close to the percolation threshold for $x = 0.20$, which grow and coalesce to form the bigger size for $x = 0.40$ resulting in a weak exchange bias effect.

PACS numbers: 75.70,Cn, 75.60.-d, 75.50.Gg

INTRODUCTION

The exchange bias (EB) coupling in a heterogeneous system gives rise to the unidirectional anisotropy at the interface when the samples are cooled down to a temperature below a critical temperature in an external magnetic field. [1] It manifests itself by a shift of the hysteresis loop and enhancement of coercivity, which attract considerable attention for the potential applications in magnetic memories, spin-electronics, and development of permanent magnet. Numerous reports are found on EB phenomenon at artificial interfaces, which have been mainly focused to develop advanced materials for the applications and understanding of the complex EB phenomenon. [2, 3, 4, 5] Nevertheless, the signature of EB phenomenon is rarely observed in compounds with a unique crystal structure and having spontaneous interface. Long back the first example of EB effect without artificial interface was reported for Cu(Mn) and Ag(Mn) alloys, which have been recognized as typical spin-glass (SG) and cluster-glass (CG) systems depending on the dilution limit. [6] Recently, the signature of EB effect has been reported at the spontaneous interfaces for few mixed-valent manganites and cobaltites with perovskite structure. [7, 8, 9, 15, 23, 24] The first report was found in a charge ordered (CO) compound $Pr_{1/3}Ca_{2/3}MnO_3$, where ferromagnetic (FM) droplets were spontaneously embedded in an antiferromagnetic (AFM) background creating the FM/AFM interface. [7] The EB phenomenon has also been reported for another CO manganite $Y_{0.2}Ca_{0.8}MnO_3$, where a strong cooling field dependence of EB is observed due to a considerable change of phase fraction between FM/AFM layers. [8] Recently, we observed the signature of EB phenomenon in the cluster-glass (CG) compounds $LaMn_{0.7}Fe_{0.3}O_3$ and $La_{0.87}Mn_{0.7}Fe_{0.3}O_3$, [9, 10] where short range FM clusters are embedded in a SG-like matrix creating spontaneous FM/SG interface. [9, 11, 12, 13] The average size of the FM clusters is found to decrease systematically with decreasing particle size, which has a strong influence on the EB phenomenon. The EB field increases significantly with decreasing particle size, which was attributed to the increase of interface area by decreasing particle size. [14] The exchange bias-like phenomenon was also reported for another CG compound, $La_{0.80}Ba_{0.20}CoO_3$, which was suggested due to the freezing effect of the local anisotropy. [15]

The mixed-valent cobaltites with perovskite structure experience the delicate interplay among charge, spin state, transport, magnetic, and structural degrees of freedom exhibiting the complex phase separation scenario. An interesting phase diagram has been proposed for the hole doped compound $Nd_{1-x}Sr_xCoO_3$ depending on the degree of hole doping. [16] For low doping range ($0 < x < 0.18$) the SG or CG state has been proposed with semiconducting temperature dependence of resistivity. With further increase in hole doping the short range FM clusters begin to coalesce above a percolation threshold ($x > 0.18$) to attain the magnetic long range ordering and start to show metallic conductivity in the ordered state. Metallic conductivity in both the paramagnetic and ordered states is observed for $x \geq 0.28$. The coexistence of ferrimagnetic (FI) and FM ordering is reported for $0.20 \leq x \leq 0.60$. Neutron powder diffraction

---

*Electronic address: sspsg2@iacs.res.in

studies on $Nd_{0.67}Sr_{0.33}CoO_3$ confirm that the FM (T_c) and FI (T_{FI}) ordering temperatures are ∼ 200 and ∼ 40 K, respectively, where ferrimagnetism was interpreted in terms of an induced antiparallel ordering of the Nd spins in close proximity of Co sublattice. [17] Several reports on electrical, magnetic, and thermodynamic studies of $Nd_{1-x}Sr_xCoO_3$ also suggest the coexistence of FI and FM ordering for $x = 0.33$ and 0.50. [18, 19, 20] ^{59}Co NMR studies on $Nd_{1-x}Sr_xCoO_3$ ($0 \leq x \leq 0.50$) confirm different spin states of Co^{3+} and Co^{4+} ions. [21] The parent compound $NdCoO_3$ shows the low spin (LS) state of Co^{3+} ion in the paramagnetic state. As a result of hole doping ($0.10 \leq x \leq 0.20$) an intermediate spin (IS) state of Co^{3+} and Co^{4+} appears in addition to the LS state of Co^{3+} and the LS state of Co^{3+} no more exists with the further increase in hole doping ($0.30 \leq x \leq 0.50$). The reported results indicate that the magnetic and electronic phase separation scenario of $Nd_{1-x}Sr_xCoO_3$ is very similar to that in $La_{1-x}Sr_xCoO_3$, where the dissimilarity is that here Nd ion carries moment unlike La ion. [22]

Recently, the signature of EB phenomenon ascribed to the intrinsic inhomogeneous phase separation was reported in the CG compounds $La_{1-x}Sr_xCoO_3$ ($0.12 \leq x \leq 0.30$), where EB was suggested due to the cluster-glass state consisting of FM and SG phases. [23, 24] In order to observe EB phenomenon the system must involve with two exchange coupled phases, the reversible and rigid phases, where magnetization of the first one can be reversed and the second one can not be. The EB is observed for $La_{1-x}Sr_xCoO_3$ at the reversible FM and rigid SG interface. The phase separated compounds $Nd_{1-x}Sr_xCoO_3$ also exhibit the necessary ingredient for the EB effect, where spontaneous phase separation between FM and FI states exists giving rise to the FM/FI interface for $x \geq 0.18$. Here, the EB phenomenon is investigated in $Nd_{1-x}Sr_xCoO_3$ with $x = 0.20$ and 0.40, where the first one is close to the percolation threshold with semiconducting behavior and the second one exhibits the metallic conductivity. We observe the EB effect for both the samples, where the effect is strong for $x = 0.20$ and weak for $x = 0.40$. In order to explain different EB effects for both the compounds the nanoscale phase separation scenario has been proposed in $Nd_{1-x}Sr_xCoO_3$ for $x \geq 0.20$. So far EB phenomenon has been reported for manganites and cobaltites with perovskite structures at spontaneous FM/AFM and FM/SG interface. Here, we present a new example of EB effect in the spontaneously phase separated compounds $Nd_{1-x}Sr_xCoO_3$ for $x \geq 0.20$, where EB effect is involved with ferrimagnetic states.

EXPERIMENTAL

The polycrystalline samples of $Nd_{1-x}Sr_xCoO_3$ with $x = 0.20$ and 0.40 were prepared by the chemical citrate route, which is described in our earlier report. [11] The stoichiometric proportion of Nd_2O_3, $SrCO_3$, and Co powders were dissolved in an aqueous solution of nitric acid, mixed thoroughly, and then citric acid was added to achieve a homogeneous mixture of the metal citrates. The metal citrates were dried and decomposed at 873 K for 6 h. Finally, the powdered samples were pressed into pellets and heated at 1273 K for 6 h followed by slow cooling at a rate of 0.7 K/min. The single orthorhombic (*Pbnm*) structure at room temperature is confirmed for both the cases, where x-ray powder diffraction (Seifert XRD 3000P) was recorded using CuK_α radiation. We do not observe any impurity phase in the x-ray diffraction patterns, which are shown in Fig. 1. The values of lattice parameters are 5.35 (a), 5.36 (b), and 7.56 (c) Å for $x = 0.20$, while for $x = 0.40$ the parameters are 5.40 (a), 5.35 (b), and 7.61 (c) Å. The lattice parameters are consistent with the earlier report. [21] The average size of the particles is found around ∼ 150.0 nm for both the cases, which was observed by a Transmission Electron Microscope (TEM), model ZEOL JEM-2010. The dc magnetization was measured using a commercial superconducting quantum interference device (SQUID) magnetometer (MPMS, XL). The sample was cooled down to the lowest temperature in zero magnetic field and the magnetization was measured in the warming cycle by applying an external magnetic field for zero-field cooled (ZFC) magnetization. On the other hand, the sample was cooled in non-zero field for the measurement of field-cooled (FC) magnetization and the measurement was performed in the warming cycle with field kept switched on.

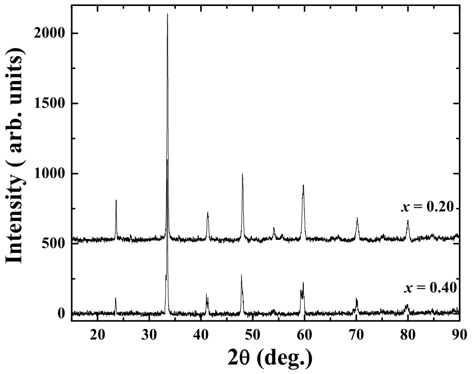

FIG. 1: X-ray powder diffraction patterns at room temperature for $Nd_{1-x}Sr_xCoO_3$ with $x = 0.20$ and 0.40.

EXPERIMENTAL RESULTS

Temperature dependence of field-cooled effect of magnetization measured at 100 Oe is shown in Fig. 2 for $Nd_{0.80}Sr_{0.20}CoO_3$. The inset of the figure exhibits ZFC magnetization highlighting the ferrimagnetic (T_{FI}) and

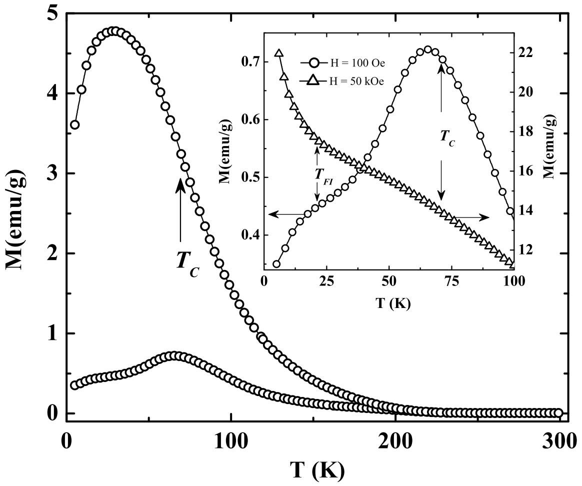

FIG. 2: Temperature dependence of magnetization measured at 100 Oe under zero field cooled (ZFC) and field cooled (FC) conditions for $x = 0.20$. The inset shows the ZFC magnetization highlighting ferrimagnetic (T_{FI}) and ferromagnetic (T_c) transitions for the measurements at 100 Oe and 50 kOe.

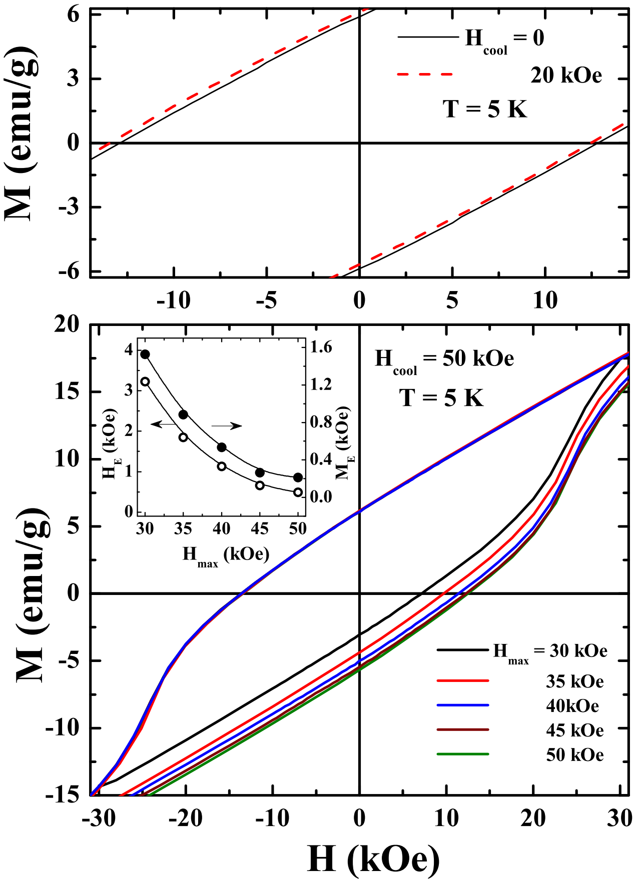

FIG. 3: (Color online) In the top panel central part of the hysteresis loops at 5 K measured after cooling the sample in zero field and field at 20 kOe, where loop measured after field cooling are indicated by the broken curve. In the bottom panel central part of the minor loops at 5 K for the measurements in between ± 30, ± 35, ± 40, ± 45, and ± 50 kOe after cooling the sample with 50 kOe. The inset exhibits the variation of exchange bias field (H_E) and magnetization (M_E) with H_{max} for $x = 0.20$.

ferromagnetic (T_c) transitions at $\sim$ 23 and $\sim$ 70 K, respectively, where T_{FI} is indicated by a shoulder around $\sim$ 23 K for the low-field measurement at 100 Oe. A sharp increase in the ZFC magnetization is observed below T_{FI} when the measurement was performed at a high field with 50 kOe. T_c is defined around $\sim$ 70 K, where a sharp increase in FC magnetization is observed for the measurement at 100 Oe. The values of T_{FI} and T_c in the present observation are reproduced exactly as compared to the values reported by Stauffer *et al.* [16] The reported experimental results including the neutron and ^{59}Co NMR results clearly indicate the coexistence of FM and FI phases at low temperature in $\mathrm{Nd}_{1-x}\mathrm{Sr}_x\mathrm{CoO}_3$ for $x \geq 0.20$. [16, 17, 18, 19, 20, 21] Thus, the magnetization loops at 5 K should have two components corresponding to the FM and FI phases. Recently, Niebieskikwiat and Salamon reported the EB effect in $\mathrm{Pr}_{1/3}\mathrm{Ca}_{2/3}\mathrm{MnO}_3$ consisting of FM and AFM phases at low temperature, where the AFM background exhibiting linear $M-H$ response was subtracted from the overall magnetization loop at 5 K to get the evident features of the horizontal and vertical shifts. [7] In the present investigation it is difficult to subtract the FI background. Nevertheless, the horizontal and vertical shifts of the hysteresis loop are clearly observed exhibiting the typical feature of EB effect when the sample was cooled in a non-zero field. For non-zero positive cooling field a negative shift in the field axis and a positive shift in the magnetization axis are observed at 5 K with respect to the hysteresis loop for $H_{cool} = 0$, which is shown in the top panel of Fig. 3. We define the coercivity, $H_C = |(H_{\mathrm{left}} - H_{\mathrm{right}})/2| \approx 13$ kOe and EB field, -$H_E = (H_{\mathrm{left}} + H_{\mathrm{right}})/2 \approx$ - 500 Oe for the measurement of magnetic hysteresis in between ± 50 kOe. Here, H_{right} and H_{left} are the positive and negative values of field at magnetization, $M = 0$, respectively. The remanence asymmetry is defined as EB magnetization (M_E), which is estimated from the vertical shifts at the saturation. [25] The value of M_E/M_S is $\sim 0.53 \times 10^{-2}$, where M_S is the saturation of magnetization. The values of the asymmetry parameters associated with the FM and FI states are comparable to those involved with the FM and SG states for the cobaltite $\mathrm{La}_{0.88}\mathrm{Sr}_{0.12}\mathrm{CoO}_3$, where the maximum effect of EB was reported in the series. [23, 24] The values of H_E and M_E/M_S were 500 Oe

Table 1: The maximum values of exchange bias field (H_E) and relative vertical shift (M_E/M_S) at different types of interfaces for phase separated cobaltites measured in between different ± H_{max}.

System	H_{max} kOe	H_E kOe	M_E/M_S (10^{-2})	Interface
$La_{0.80}Ba_{0.20}CoO_3$[15]	3	0.54	-	FM/SG
$La_{0.88}Sr_{0.12}CoO_3$[26]	20	2.95	10.40	FM/SG
$La_{0.88}Sr_{0.12}CoO_3$[24]	50	0.50	1.10	FM/SG
$Nd_{0.80}Sr_{0.20}CoO_3$*	30	3.23	4.15	FM/SG
	50	0.50	0.53	FM/FI
$Nd_{0.60}Sr_{0.40}CoO_3$*	50	0.08	0.55	FM/FI

* Current investigation

and 1.10 × 10^{-2}, respectively when hysteresis was measured in between ± 50 kOe for $La_{0.88}Sr_{0.12}CoO_3$. [24] The reported values of the shifts for the phase separated cobaltites are compared in Table 1 with the present observations for $x = 0.20$ and 0.40 for different H_{max}, where H_{max} is the maximum field used for the measurement of hysteresis loops.

The characteristics of EB phenomenon strongly depend on the delicate interplay among Zeeman energy (E_Z) associated with the FM clusters, anisotropy energy (E_A) associated with the FI clusters, and exchange energy (E_{ex}) at the FM/FI interface. The first term can be experimentally controlled by tuning H_{cool} and H_{max}. The magnetic hysteresis loops were measured for $x = 0.20$ at 5 K in between $\pm H_{max}$ = ± 30, ± 35, ± 40, ± 45, and ± 50 kOe when the sample was cooled down to 5 K from 250 K in presence of 50 kOe field. The central parts of the hysteresis loops are shown in the bottom panel of Fig. 3. The values of H_E and M_E as a function of H_{max} are shown in the inset of the figure. The values of H_E and M_E are decreased with increasing H_{max}. The plots further indicate that the values show a tendency of stabilization for $H_{max} \geq 45$ kOe. We note that the hysteresis loops measured in between ± 45 and ± 50 kOe almost merge together. The H_{max} dependence of H_E and M_E has been reported by Tang *et al.* for $La_{0.82}Sr_{0.18}CoO_3$, where H_E and M_E vanish even at small value of H_{max} = 30 kOe. [23] The results are analogous to the minor loops effect, which is explicitly described by Geshev. [27] However, the signature of EB effect in $La_{0.82}Sr_{0.18}CoO_3$ was confirmed by the training effect. [23] The H_{max} dependence of H_E and M_E has also been investigated by Salazar-Alvarez *et al.* for MnO/Mn_3O_4 core/shell structure, where the plots show the non-zero asymptotic value of the horizontal shift while the vertical shifts virtually vanish at $H_{max} > 70$ kOe. [28] In the present observation the plots show that H_E and M_E stabilize around H_{max} = 50 kOe, where the values of H_E and M_E are considerably large. The results indicate that the plots are not the typical minor loops effect described by Geshev [27], rather it exhibits significant EB effect.

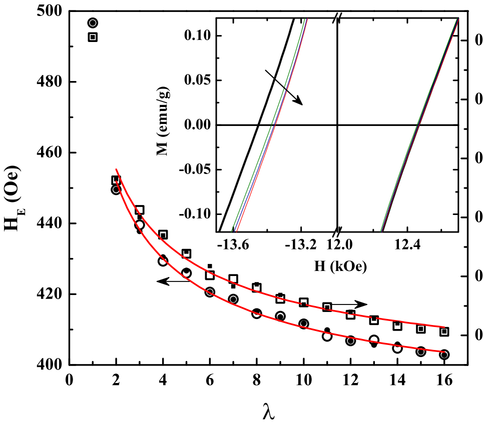

FIG. 4: (Color online) The decrease of exchange bias field (H_E) and magnetization (M_E) with the consecutive number (λ) of cycling of the hysteresis loop for $x = 0.20$ exhibiting training effect. The central part of the 1st, 2nd, 8th, and 16th loops are shown in the inset, where arrow indicates the increasing direction of λ.

Training effect is one of the important features of the exchange bias system, which describes the decrease of H_C, H_E, and M_E when the system is successively field cycled at a particular temperature after the field cooling. [4, 7, 23] The training effect is investigated for x = 0.20, where the sample was cooled down to 5 K from 250 K in presence of 20 kOe field and then the hysteresis loops were measured successively in between ± 50 kOe up to 16 times. We note that the training effect is evident in the system. The central parts of the 1st, 2nd, 8th, and 16th loops are shown in the inset of Fig. 4. The systematic decrease of H_E and M_E with the consecutive cycling number (λ) are shown in Fig. 4 by the open symbols. The values of H_E and M_E are decreased up to ∼ 10 % and ∼ 11 %, respectively for $\lambda = 2$, which are comparable to the reported results for the spontaneously phase separated systems. For $Pr_{1/3}Ca_{2/3}MnO_3$ [7] bearing the FM/AFM interface the value of M_E was decreased up to ∼ 20 % for the second cycle, whereas the values of M_E and H_E were decreased up to ∼ 10 % and ∼ 19 %, respectively for $La_{0.82}Sr_{0.18}CoO_3$ having FM/SG interface. [23]

The decrease of H_E (M_E) is fitted satisfactorily with the following empirical relation

$$H_E(\lambda) - H_E^{\infty} \propto \frac{1}{\sqrt{\lambda}}, \qquad (1)$$

where H_E^{∞} is the value for $\lambda \to \infty$. The solid lines in Fig. 4 exhibit the best fit of H_E and M_E variation with λ for $\lambda \geq 2$. The values of the fitted parameters are $H_E^{\infty} \approx$ 377 Oe and $M_E^{\infty} \approx 0.157$ emu/g. The above empirical relation does not fit the sharp decrease between first and

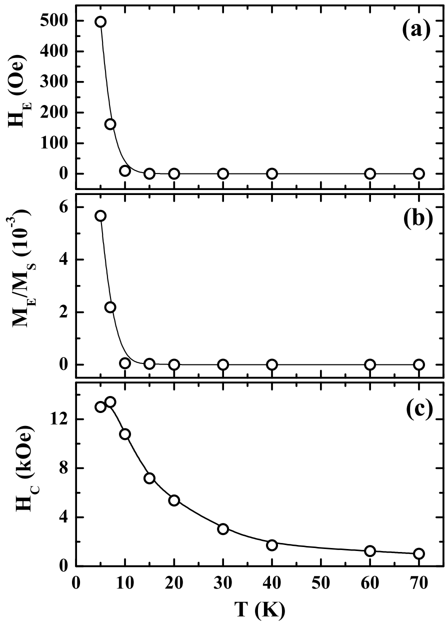

FIG. 5: Temperature dependence of (a) exchange bias field (H_E), (b) relative vertical shift (M_E/M_S), and (c) coercivity (H_C) with H_{cool} = 20 kOe for x = 0.20.

second loops, which is in accordance with the reported results. [4, 7, 23] Recently, Binek proposed a recursive formula in the framework of spin configurational relaxation to understand the training effect for a FM/AFM heterostructure, which describes the (λ+1)th loop shift with respect to the λth one as [29]

$$H_E(\lambda+1) - H_E(\lambda) = -\gamma[H_E(\lambda) - H_E^{\infty\prime}]^3, \qquad (2)$$

where γ is a sample dependent constant. Using $\gamma = 2.28 \times 10^{-5}$ Oe^{-2} and $H_E^{\infty\prime} = 369.4$ Oe the whole set of data is reproduced for H_E, while the values of γ and $M_E^{\infty\prime}$ are 79.5 (emu/g)$^{-2}$ and 0.153 emu/g, respectively for M_E. The calculated values are shown by the filled symbols in Fig. 4, which matches satisfactorily with the experimental data (open symbols). Thus, the spin configurational relaxation model can describe our experimental results satisfactorily, where successive reversal of the FM spins triggers the configurational relaxation of the interfacial FI spins toward equilibrium giving rise to the training effect.

The magnetic hysteresis loops were measured in between ± 50 kOe at different temperatures for $Nd_{0.80}Sr_{0.20}CoO_3$ with the sample been cooled down to the desired temperatures from 250 K with H_{cool} = 20 kOe. The values of H_C, H_E, and M_E/M_S as a function of temperature are shown in Fig. 5. H_C decreases slowly and vanishes at the onset of the Curie temperature around ∼ 70 K. On the other hand, H_E and M_E/M_S decrease sharply with increasing temperature and disappear for $T \geq 20$ K, where a shoulder in the ZFC magnetization is observed indicating the signature of ferrimagnetic ordering. The temperature dependence of the asymmetry parameters are typical for the exchange biased systems viz., charge ordered $Pr_{1/3}Ca_{2/3}MnO_3$, [7] cluster-glass $LaMn_{0.7}Fe_{0.3}O_3$, [9] and cluster-glass cobaltites $La_{1-x}Sr_xCoO_3$, [23, 24] where EB effect vanishes above AFM (T_N) or spin freezing (T_f) transition temperature. In the cases of EB systems the rigid AFM or SG spins apply a coupling force on the FM spins at the interface and a layer of pinned or frozen FM spins are created on the outer surface of the FM clusters when the system is cooled in non-zero field. The pinned or frozen FM spins give rise to the unidirectional shift of the hysteresis loops and reveal the EB effect. For $Nd_{1-x}Sr_xCoO_3$ with $x \geq 0.20$ the coexistence of FM and FI phases has been suggested by Stauffer *et al.*, [16] which is also indicated here by the ZFC magnetization for x = 0.20 (inset of Fig. 2). Therefore, the EB effect below T_{FI} is suggested due to the pinning effect. The rigid FI spins operate the pinning force on the reversible FM spins at the FM/FI interface and the pinned FM spins lead to the EB effect. The signature of EB effects involving with the ferrimagnetic phase are reported at the different combinations of artificial interfaces viz., FM/FI, FI/AFM, and FI/FI interface for different bilayer heterogeneous structures. [4, 28, 30, 31, 32, 33] Here, we observe the new results of EB effect at the intrinsic FM/FI interface, where the EB effect is ascribed to the spontaneous separation between FM and FI phases.

The cooling field dependence of EB effect was investigated for x = 0.20, where the sample was cooled down to 5 K from 250 K with different cooling fields and the hysteresis loops were measured in between ± 50 kOe. The H_{cool} dependence of H_E is shown in the top panel of Fig. 6. The value of H_E increases sharply with H_{cool} up to 10 kOe and then shows a slight decreasing trend above 20 kOe. As seen in the inset of the top panel of the figure the H_{cool} dependence of H_C follows similar behavior like the H_{cool} dependence of H_E, where the sharp increase of H_C is associated with the increase of H_E. The plots of H_E and H_C with H_{cool} exhibit that it follows nearly linear dependence above 20 kOe, which is shown in Fig. 7. Recently, Qian *et al.* have shown the linear H_{cool} dependence of H_E above 10 kOe, where strong correlation between H_E and H_C was reported. [8] The authors further suggested that the decrease of H_E with increasing H_{cool} is associated with the increase of the size of the FM layers for $Y_{0.2}Ca_{0.8}MnO_3$. Considering the magnetization at 50 kOe close to the saturation value at 5 K, the increase of M_{50} indicates the increase of the average size of the FM clusters, where M_{50} is determined from the average value of the positive and negative values of the magnetization at 50 kOe. The linear plot of H_E against M_{50}^{-1} is shown in the inset of Fig. 7, which indicates that H_E is inversely

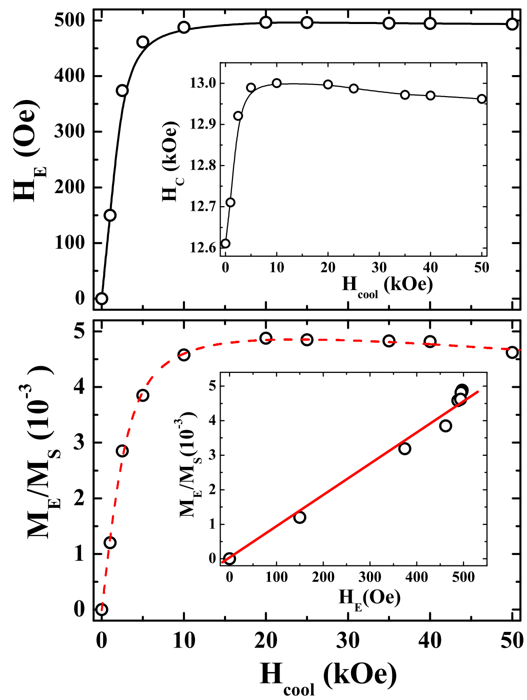

FIG. 6: (Color online) Cooling field (H_{cool}) dependence of (top panel) exchange bias field (H_E) and (bottom panel) M_E/M_S at 5 K for $x = 0.20$, where the hysteresis loops were measured between ± 50 kOe. M_E and M_S are the exchange bias magnetization and saturation magnetization. The H_{cool} dependence of coercivity (H_C) and the plot of M_E/M_S against H_E are shown in the inset of top and bottom panels, respectively. The broken curve in the bottom panel is the fitted curve using simplified exchange interaction model. The solid straight line in the inset of the bottom panel shows the linear fit.

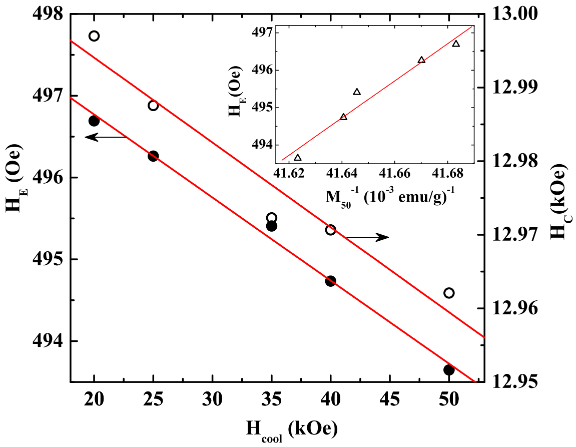

FIG. 7: (Color online) Plots of exchange bias field (H_E) and coercivity (H_C) against cooling field (H_{cool}) at 5 K for $x = 0.20$. Inset shows the plot of H_E as a function of inverse of the average magnetization at 50 kOe (M_{50}^{-1}). Solid straight lines indicate the linear fits.

proportional to the size of the FM clusters. Note that a very small decrease of H_E around ∼ 0.6 % is observed at 5 K for the increase of H_{cool} from 20 kOe to 50 kOe. In the high H_{cool} range the feature of H_E is reminiscent to that observed for FM/AFM bilayers, [34] AFM-core and FI-shell structure, [28] and unlike to that observed for FM/SG systems. [9, 14, 23, 24, 35] For the exchange biased systems involved with a SG state the values of H_E are decreased considerably with increasing H_{cool} above a certain value of H_{cool}, where large H_{cool} typically affects the frozen spins in the SG phase and frozen FM spins by polarizing the glassy magnetic spins toward the direction of H_{cool}. In fact, H_E decreases up to ∼ 40 % for the increase of H_{cool} from 20 to 50 kOe in $La_{0.88}Sr_{0.12}CoO_3$, [24] ∼ 47 % for the increase of H_{cool} from 6 to 12 kOe in $LaMn_{0.7}Fe_{0.3}O_3$, [9] and ∼ 25 % for the increase of H_{cool} from 2 to 4 kOe in $La_{0.87}Mn_{0.7}Fe_{0.3}O_3$, [10] where the systems are involved with the SG states exhibiting EB effect. The frozen FM spins and pinned FM spins may have different features of cooling field dependence, where the large values of H_{cool} can not influence the pinned FM spins significantly, which is indicated by the minor change of H_E for AFM or FI state. The large reduction of H_E around ∼ 37 % is exceptionally observed in $Y_{0.2}Ca_{0.8}MnO_3$ for the increase of H_{cool} from 10 kOe to 60 kOe, which is associated with the FM/AFM interface. In the above case the large decrease of H_E was attributed to the increase of the phase fraction of the FM layer at the cost of AFM layer, which was pointed out by Qian *et al.* [8] Herein, the minor reduction of H_E around ∼ 0.6 % may indicate that small increase of the size of FM clusters is ascribed to the reduction of pinned FM layers at the FM/FI interface, which does not involve with the conversion of phase fraction.

Recently, a simplified exchange interaction model has been proposed by Niebieskikwiat and Salamon considering the FM clusters to be embedded in the AFM host for charge ordered compound $Pr_{1/3}Ca_{2/3}MnO_3$. [7] The FM clusters were assumed to have a single domain structure, which exhibit magnetization reversal like FM nanoparticles consisting of single magnetic domain. The model gives the simplified relation between H_E and M_E/M_S as $H_E \propto M_E/M_S$ for $\mu H_E < k_BT$, where M_S and μ are the saturation magnetization and average moment of the FM clusters, respectively. We observe nearly linear behavior between H_E and M_E/M_S in the inset of the bottom panel of Fig. 6, which has also been verified for $Pr_{1/3}Ca_{2/3}MnO_3$, [7] $CaMnO_{3-\delta}$, [36] $LaMn_{0.7}Fe_{0.3}O_3$, [9, 14] and $La_{0.87}Mn_{0.7}Fe_{0.3}O_3$ [10] exhibiting the EB effect. Here, the value of $\mu H_E/k_BT \approx 0.87$, where the value of μ is obtained from the fit of M_E/M_S against

H_{cool} plot, which is described below. Note that the value of $\mu H_E/\text{k}_B T$ was ~ 0.9 for $\text{Pr}_{1/3}\text{Ca}_{2/3}\text{MnO}_3$. [7] The linear dependence of the M_E/M_S against H_E plot indicates that FM clusters may have a single domain structure for $\text{Nd}_{0.80}\text{Sr}_{0.20}\text{CoO}_3$. The model further defines the H_{cool} dependence of M_E/M_S as

$$H_E \propto M_E/M_S \propto j_i \left[\frac{j_i \mu_0}{(g\mu_B)^2} L\left(\frac{\mu H_{cool}}{k_B T_f}\right) + H_{cool} \right], \quad (3)$$

which was verified successfully for spontaneously phase separated $\text{Pr}_{1/3}\text{Ca}_{2/3}\text{MnO}_3$, [7] $\text{LaMn}_{0.7}\text{Fe}_{0.3}\text{O}_3$, [9, 14] and $\text{La}_{0.87}\text{Mn}_{0.7}\text{Fe}_{0.3}\text{O}_3$. [10] The first term in the expression dominates for small H_{cool}, whereas the second term dominates for large H_{cool}, which varies linearly with H_{cool}. In the above relation J_i and μ are adjustable parameters, where J_i is the interface exchange constant. T_f in the above expression was defined as the freezing temperature below which M_E/M_S was found to increase steeply for $\text{Pr}_{1/3}\text{Ca}_{2/3}\text{MnO}_3$. Here, we assume the value of $T_f \sim 15$ K below which M_E/M_S increases sharply. The broken curve in the bottom panel of Fig. 6 exhibits a satisfactory fit of the experimental data using the above expression. The number density of FM clusters (n) is estimated from the saturation magnetization, $M_S \approx n\mu$, where the value of M_S at 5 K is obtained from the extrapolation of the magnetization to $1/H \rightarrow 0$. The value of n is $\approx 15.5 \times 10^{-5}$ Å^{-3} which further gives the rough estimate of the size of the FM clusters around ~ 20 Å. The value of the size of FM cluster is consistent with those around ~ 10 Å for $\text{Pr}_{1/3}\text{Ca}_{2/3}\text{MnO}_3$ [7] and ~ 10 - 30 Å for $\text{LaMn}_{0.7}\text{Fe}_{0.3}\text{O}_3$ depending on the particle size. [14]

We also investigate the EB effect for $x = 0.40$, where the maximum values of H_E and M_E/M_S are shown in Table 1. The value of M_E/M_S is nearly the same, whereas H_E is much smaller for $x = 0.40$ than that of the value for $x = 0.20$. The H_{cool} dependence of EB effect was also measured for $x = 0.40$. The plots of H_E and M_E/M_S as a function of H_{cool} at 5 K are shown in Fig. 8. H_E is found to increase sharply up to ~ 20 kOe and shows a decreasing trend with the further increase of H_{cool}, where M_E/M_S follows almost similar behavior. The linear dependence of M_E/M_S against H_E is observed for $x = 0.40$ analogous to $x = 0.20$, which indicates that the FM clusters of $x = 0.40$ also have a single domain structure. We observe the linear H_{cool} dependence of H_E and H_C above 20 kOe, which is shown in the inset of Fig. 8. Here, a very small decrease of H_E (~ 0.5 %) is also observed for $x = 0.40$ like $x = 0.20$. The model proposed by Niebieskikwiat and Salamon [7] was used to fit the H_{cool} dependence of M_E/M_S, where the satisfactory fit is shown in Fig. 8 by the broken curve. The number density of FM clusters is thus obtained from the fit as $n \approx 32.5 \times 10^{-5}$ Å^{-3}, which gives the rough estimate of the size of the FM clusters around ~ 40 Å. The analysis indicates that the average size of the FM clusters is increased considerably for $x = 0.40$ than $x = 0.20$.

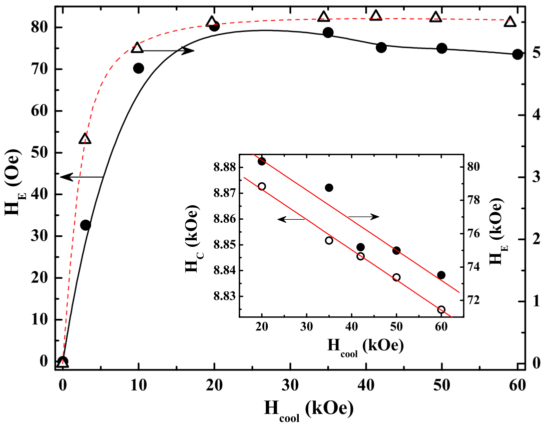

FIG. 8: (Color online) Plots of exchange bias field (H_E) and relative vertical shift (M_E/M_S) against cooling field (H_{cool}) at 5 K for $x = 0.40$. The broken curve is the fit of the H_{cool} dependence of M_E/M_S plot. Inset shows the plot of H_E and H_C as a function of H_{cool}. Solid straight lines indicate the linear fits.

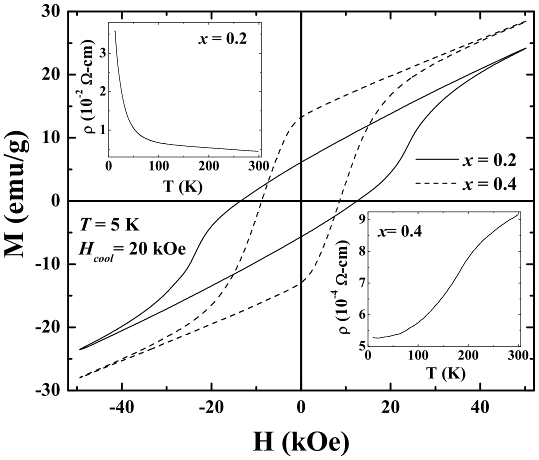

FIG. 9: Magnetic hysteresis loop at 5 K after field cooling with 20 kOe for $x = 0.20$ (continuous curve) and $x = 0.40$ (broken curve) for $\text{Nd}_{1-x}\text{Sr}_x\text{CoO}_3$. The upper and lower insets exhibits the temperature dependence of resistivity (ρ) for $x = 0.20$ and 0.40, respectively.

Temperature variation of resistivity (ρ) for the samples with $x = 0.20$ and 0.40 are shown in the upper and lower insets of Fig. 9, respectively. The semiconducting temperature dependence of ρ is observed for $x = 0.20$, while for $x = 0.40$ nearly linear temperature dependence of ρ is observed in the paramagnetic state and a sharp decrease of ρ is observed below T_C at 200 K. Temperature dependence of ρ for both the samples are similar to the reported results [16] except for the magnitude of ρ. The slightly larger values of the resistivity in the present investigations might be attributed to the particle size effect, where the particle size in the present observation ($\sim$ 150 nm) is less than that of the results reported by Stauffer *et al.* [16] For $x = 0.20$ the system is close to the percolation limit, where the hole rich FM clusters are of small size, which grow and coalesce with increasing x. Therefore, the average size of the FM clusters for $x = 0.40$ is larger than that of the sample with $x = 0.20$, which is reflected in the temperature dependence of resistivity and the analysis of the H_{cool} dependence of M_E/M_S. The size of the FM clusters is also crucial for the EB effect. The hysteresis loops measured at 5 K under identical condition with $H_{cool} = 20$ kOe are shown in Fig. 9 for $x = 0.20$ and 0.40. The values of H_E and M_E/M_S are 82 Oe and 0.55×10^{-2} for $x = 0.40$, while for $x = 0.20$ the values are 500 Oe and 0.53×10^{-2}, respectively (see Table 1). In addition, the magnetization at 50 kOe and H_C are 28.55 emu/g and 8.7 kOe for $x = 0.40$, and 23.92 emu/g and 13.0 kOe for $x = 0.20$, respectively. The values of magnetization at 50 kOe indicate that the size and density of the FM clusters are increased for $x = 0.40$ compared to $x = 0.20$, which is reflected in H_E, where H_E is much smaller for $x = 0.40$. Similar features of EB effect was observed for the particle size dependence of EB phenomenon in the cluster-glass compound $\mathrm{LaMn_{0.7}Fe_{0.3}O_3}$, where FM clusters are embedded in the SG matrix. [14] The sizes of the FM clusters were found to increase with increasing particle size, which resulted in a decrease in the EB effect. Negligible EB effect was observed for the particles with average size $\sim$ 300 nm. The increase of the size of the FM clusters decreases the effective interface area, which might be the origin of weakening of the effective exchange coupling at the FM/FI interface in the present investigations. The explanation is consistent with the model proposed by Meiklejohn, which predicts the relation, $H_E \approx J_{ex}/(M_{FM} \times t_{FM})$, where J_{ex} is the exchange constant across the FM/AFM interface per unit area. [37] M_{FM} and t_{FM} are the magnetization and the thickness of the FM layer, respectively. The increase of M_{FM} and t_{FM} in the denominator of the above expression decreases the EB field. In the present investigation the average size of the FM clusters, analogous to t_{FM}, is increased for $x = 0.40$ compared to $x = 0.20$, which results in the decrease of EB field.

SUMMARY

As none before, we observe the signature of exchange bias effect in $\mathrm{Nd_{1-x}Sr_xCoO_3}$ for $x = 0.20$ and 0.40 at the spontaneous ferromagnetic/ferrimagnetic interface. When the sample was cooled in a static magnetic field, the systematic shifts of the magnetic hysteresis loops are observed as a function of temperature and cooling field. The exchange bias effect vanishes above the ferrimagnetic transition (T_{FI}) temperature, which indicates that the ferrimagnetic spins apply a pinning force on the reversible ferromagnetic spins at the interface below T_{FI} and the pinned ferromagnetic spins give rise to the exchange bias phenomenon. The exchange bias is further confirmed by the training effect, which could be explained satisfactorily by the spin configurational relaxation model. The exchange bias field is found to increase sharply ($\leq$ 10 kOe) with increasing cooling field and then it shows a very small decreasing trend ($\geq$ 20 kOe) for high cooling field. The coercivity almost follows a similar trend of exchange bias field, where a linear dependence of exchange bias field and coercivity against cooling field is observed above 20 kOe for both the compounds. The cooling field dependence of exchange bias effect is analysed by the simplified exchange interaction model, which gives a rough estimate of the average size of the ferromagnetic clusters around $\sim$ 20 and $\sim$ 40 Å, where the FM clusters consisting of single magnetic domain are suggested for x = 0.20 and 0.40, respectively. The sizes of the ferromagnetic clusters are close to the percolation threshold for x = 0.20, which grow and coalesce with increasing x. The large size of the ferromagnetic clusters leads to the weak exchange bias effect for $x = 0.40$.

One of the authors (S.G.) wishes to thank DST (Project No. SR/S2/CMP-46/2003), India for the financial support. The particle size of the samples were measured by TEM under the scheme of Nanoscience and Nanotechnology initiative of DST at IACS, Kolkata, India. The authors wish to thank Mr. A. Karmakar for the English corrections. M.P. also wishes to thank CSIR for the JRF fellowship.

[1] W. H. Meiklejohn and C. P. Bean, Phys. Rev. **102**, 1413 (1956).

[2] R. L. Stamps, J. Phys. D: Appl. Phys. **33**, R247 (2000).

[3] M. Kiwi, J. Magn. Magn. Mater. **234**, 584 (2001).

[4] J. Nogues, J. Sort, V. Langlais, V. Skumryev, S. Surinach, J. S. Munoz, and M. D. Baro, Physics Reports **422**, 65 (2005); J. Nogues, J. Sort, V. Langlais, V. Skumryev, S. Surinach, J. S. Munoz, and M. D. Baro, Int. J. Nanotechnology **2**, 23 (2005); J. Nogues and I. K. Schuller, J. Magn. Magn. Mater. **192**, 203 (1999).

[5] A. E. Berkowitz and K. Takano, J. Magn. Magn. Mater. **200**, 552 (1999).

[6] J. S. Kouvel, J. Phys. Chem. Solids **21**, 57 (1961).

[7] D. Niebieskikwiat and M. B. Salamon, Phys. Rev. B **72**, 174422 (2005).

[8] T. Qian, G. Li, T. Zhang, T. F. Zhou, X. Q. Xiang, X. W. Kang, and X. G. Lia, Appl. Phys. Lett. **90**, 012503 (2007).

[9] M. Patra, K. De, S. Majumdar, and S. Giri, Eur. Phys.

J. B **58**, 367 (2007).

[10] K. De, M. Patra, S. Majumdar, and S Giri, J. Phys. D: Appl. Phys. **41**, 175007 (2008).

[11] K. De, R. Ray, R. N. Panda, S. Giri, H. Nakamura, and T. Kohara, J. Magn. Magn. Mater. **288**, 339 (2005).

[12] K. De, M. Patra, S. Majumdar, and S. Giri, J. Phys. D: Appl. Phys. **40**, 7614 (2007).

[13] X. J. Liu, Z. Q. Li, A. Yu, M. L. Liu, W. R. Li, B. L. Li, P. Wu, H. L. Bai, and E. Y. Jiang, J. Magn. Magn. Mater. **313**, 354 (2007).

[14] M. Thakur, M. Patra, K. De, S. Majumdar, and S. Giri, J. Phys. Condensed Matter. **20**, 195215 (2008).

[15] W. Luo and F. Wang, Appl. Phys. Lett. **90**, 162515 (2007).

[16] D. D. Stauffer and C. Leighton, Phys. Rev. B **70**, 214414 (2004).

[17] A. Krimmel, M. Reehuis, M. Paraskevopoulos, J. Hemberger, and A. Loidl, Phys. Rev. B **64**, 224404 (2001).

[18] M. Paraskevopoulos, J. Hemberger, A. Krimmel, and A. Loidl, Phys. Rev. B **63**, 224416 (2001).

[19] K. Yoshii, A. Nakamura, H. Abe, M. Mizumaki, and T. Muro, J. Magn. Magn. Mater. **239**, 85 (2002); K. Yoshii and H. Abe, Phys. Rev. B **67**, 094408 (2003).

[20] A. Fondado, M. P. Breijo, C. Rey-Cabezudo, M. Sanchez-Andujar, J. Mira, J. Rivas, and M. A. Senaris-Rodriguez, J. Alloys Compd. **323324**, 444 (2001).

[21] A. Ghoshray, B. Bandyopadhyay, K. Ghoshray, V. Morchshakov, K. Barner, I. O. Troyanchuk, H. Nakamura, T. Kohara, G. Y. Liu and G. H. Rao, Phys. Rev. B **69**, 064424 (2004).

[22] J. Wu and C. Leighton, Phys. Rev. B **67**, 174408 (2003).

[23] Y. K. Tang, Y. Sun, and Z. H. Cheng, Phys. Rev B **73**, 174419 (2006).

[24] Y. K. Tang, Y. Sun, and Z. H. Cheng, J. Appl. Phys. **100**, 023914 (2006).

[25] J. Nogués, C. Leighton, and Ivan K. Schuller, Phys. Rev. B **61**, 1315 (2000).

[26] M. Patra, S. Majumdar, and S. Giri (unpublished).

[27] J. Geshev, J. Magn. Magn. Mater. **320**, 600 (2008).

[28] G. Salazar-Alvarez, J. Sort, S. Suriñach, M. D. Baró, and J. Nogués, J. Am. Chem. Soc. **129**, 9102 (2007).

[29] C. Binek, Phys. Rev. B **70**, 014421 (2004).

[30] F. Canet, S. Mangin, C. Bellouard, and M. Piecuch, Europhys. Lett. **52**, 594 (2000).

[31] S. Mangin, F. Montaigne, and A. Schuhl, Phys. Rev. B **68**, 140404(R) (2003).

[32] A. E. Berkowitz, G. F. Rodriguez, J. I. Hong, K. An, T. Hyeon, N. Agarwal, D. J. Smith, and E. E. Fullerton, Phys. Rev. B **77**, 024403 (2008).

[33] T. Hauet, J. A. Borchers, P. Mangin, Y. Henry, and S. Mangin, Phys. Rev. Lett. **96**, 067207 (2006).

[34] J. W. Cai, Kai Liu, and C. L. Chien, Phys. Rev. B **60**, 72 (1999).

[35] L. DelBianco, D. Fiorani, A. M. Testa, E. Bonetti, and L. Signorini, Phys. Rev. B **70**, 052401 (2004); D. Fiorani, L. Del Bianco, A. M. Testa and K. N. Trohidou, J. Phys.: Condens. Matter **19**, 225007 (2007).

[36] V. Markovich, I. Fita, A. Wisniewski, R. Puzniak, D. Mogilyansky, L. Titelman, L. Vradman, M. Herskowitz, and G. Gorodetsky, Phys. Rev. B **77**, 054410 (2008).

[37] W. H. Meiklejohn, J. Appl. Phys. **33**, 1328 (1962).